Chen *et al. J Mater Inf* 2023;3:10
DOI: 10.20517/jmi.2023.06

Journal of Materials Informatics

Review

Open Access

Data-driven design of eutectic high entropy alloys

Zhaoqi Chen[1], **Yong Yang**[1,2,3,*]

[1]Department of Mechanical Engineering, City University of Hong Kong, Hong Kong 999077, China.
[2]Department of Materials Science and Engineering, City University of Hong Kong, Hong Kong 999077, China.
[3]Department of Advanced Design and System Engineering, City University of Hong Kong, Hong Kong 999077, China.

[*]**Correspondence to:** Prof. Yong Yang, Department of Mechanical Engineering, City University of Hong Kong, Tat Chee Avenue, Kowloon Tong, Kowloon, Hong Kong 999077, China. E-mail: yonyang@cityu.edu.hk

How to cite this article: Chen Z, Yang Y. Data-driven design of eutectic high entropy alloys. *J Mater Inf* 2023;3:xx. https://dx.doi.org/10.20517/jmi.2023.06

Received: 2 Feb 2023 **First Decision:** 3 Mar 2023 **Revised:** 18 Mar 2023 **Accepted:** 6 Apr 2023 **Published:** 28 Apr 2023

Academic Editor: Xingjun Liu **Copy Editor:** Ke-Cui Yang **Production Editor:** Ke-Cui Yang

Abstract

Eutectic high entropy alloys (EHEAs) have attracted tremendous research interest over the past decade due to their superior physical and mechanical properties. Given the compositional complexity, there are no well-established phase diagrams for EHEAs. Therefore, the compositional design of EHEAs has been following a trial-and-error empirical approach, which is time-consuming, costly, and ineffective. To accelerate the search for EHEAs, data-driven approaches, particularly machine learning (ML) based modeling, have recently been utilized in lieu of the traditional empirical approach. In this article, we provide a critical overview of the recent efforts in the design and development of EHEAs, which covers the various empirical methods and the state-of-the-art machine learning models developed for EHEAs. In addition, we also briefly discuss the mechanical properties and plasticity strengthening mechanisms in EHEAs which are related to their heterogeneous microstructure, such as heterogeneous deformation induced strengthening, twinning induced strengthening, and phase transformation induced strengthening.

Keywords: Eutectic alloys, high entropy alloys, machine learning, alloy design, mechanical properties

INTRODUCTION

Eutectic alloy, in which at least two phases form and grow in a coupled manner during solidification, has attracted immense attention and interest in both academia and industries in past decades[1,2]. The term

"eutectic" was coined by Guthrie in 1884 to refer to easy melt (i.e., the minima on a liquidus curve)[3]. Since the melting temperature of a eutectic alloy is always lower than those of its constituent phases, eutectic alloys often exhibit good castability. Additionally, their eutectic microstructures can be readily tailored through thermomechanical processing for optimized properties, such as high rupture strength[4-6], good high-temperature creep resistance[7-9], high thermal conductivity[10,11] and superior wear and corrosion resistance[12-15]. Compared to single-phase alloys, eutectic alloys usually possess balanced mechanical properties that can meet demanding requirements in structural applications[1,16-18].

To date, a number of eutectic alloy systems have already been developed for various applications, such as Sn-Pb as solder joints[19-21], Sn-Ag for electronics[22-24], Ni-Si for magnetics[25,26], In-Ga for optics[27,28] and Ni-Al-Cr for aerospace engineering[29,30]. However, just like many other conventional alloys, the design of conventional eutectic alloys is usually based on one principal element. If the phase diagram is not available, alloying elements are then added in a trial-and-error manner to pinpoint a eutectic composition. While people have been following such a design strategy for decades, this approach is costly, time-consuming, and inefficient, particularly when it comes to compositionally complex alloys (CCAs), such as multi-principal-element alloys (MPEAs)[31-33] and high entropy alloys (HEAs)[34,35], for which there is no phase diagram and the associated compositional space is too broad to navigate with the traditional design strategy.

In the past, the development of HEAs in their infancy was mainly focused on the formation of single-phase solid solutions[36-41], while the recent trend has shifted to multi-phase HEAs with balanced mechanical properties[42-44]. One good example is the so-called eutectic high entropy alloys (EHEAs) comprising a biphasic or triphasic microstructure with a lamellar or rod morphology[1,45]. By carefully controlling the thermal and mechanical processing, EHEAs can exhibit a wide range of microstructural feature sizes, ranging from tens of nanometers to a few microns[46-49]. Owing to these heterogeneous eutectic micro- or nanostructures, EHEAs can attain high strength and good ductility[46,47,50,51], remarkable creep resistance[45,52], superior thermal stability at elevated temperatures[53-55] and good processability[56].

Given the vast hyper-dimensional compositional space for EHEAs, the traditional design strategy becomes impractical. Therefore, several design methods were proposed recently to quickly locate the possible eutectic or near-eutectic composition in the compositional space. These include, the simple mixing method[57-60], the grouping method[61-63], the pseudo-binary methods[64-67] and the so-called "LEGO" method[68]. The pros and cons of these methods are listed in Table 1 and they can be categorized into two strategies, as summarized in Figure 1. However, we note that these methods are mostly empirical; therefore, the related experimental workload that one has to pay is heavy to verify these empirical predictions as the number of constituent elements increases. To improve efficiency, people usually turned to machine learning (ML) as an alternative to the traditional design strategy for the development of advanced alloys (i.e., titanium alloys[69,70], copper alloys[71,72], shape memory alloys[73-75] and even metallic glasses[76-78]). Recently, these efforts were extended to the design of EHEAs[79-81]. In the present work, we provide a critical overview of these recent efforts for the development of EHEAs covering the empirical design methods and the data-driven methods.

EMPIRICAL DESIGN METHODS OF EUTECTIC HIGH ENTROPY ALLOYS

Linear combination of binary eutectics

Without a phase diagram, it is non-trivial and difficult to locate the eutectic compositions for multi-component alloys and HEAs. Therefore, to facilitate the design of EHEAs, one strategy is to resort to the phase diagrams of binary eutectics, which can be easily found in the literature[57,59,60,68]. In other words, there is a hypothesis that the eutectic microstructures of multi-component systems may inherit from some binary/ternary eutectics[68,82,83]. While this hypothesis remains to be verified theoretically, it indeed provides

Table 1. Pros and cons of the empirical methods for EHEA design

Methods	Pros	Cons
Simple mixing method	Take binary eutectics as the constituents, which can be easily located from phase diagrams	(1) Lack of supportive physical and thermodynamic theories, which significantly reduces the efficiency
"LEGO" method		
Pseudo-binary method	With the help of CALPHAD, a pseudo-binary system can be quickly constructed and evaluated	(2) The explorable space following empirical methods is limited compared with the vast compositional space of HEAs
Grouping method		

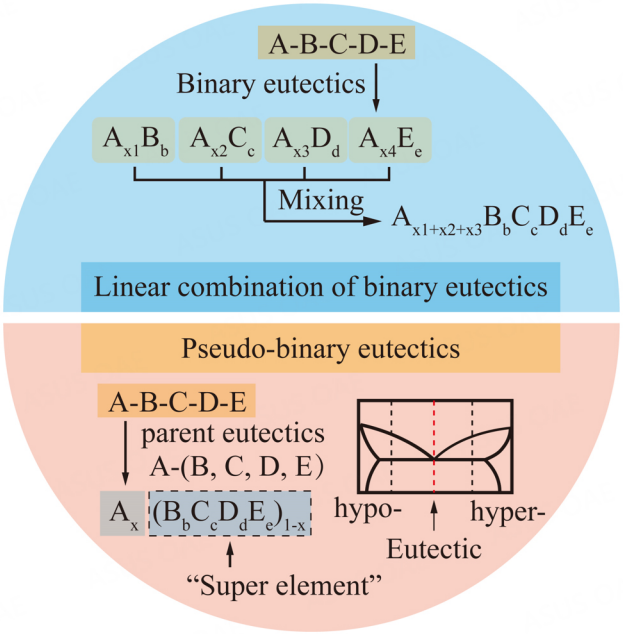

Figure 1. The schematic for the various empirical design methods for eutectic high entropy alloys.

an avenue to locate EHEA compositions. In practice, one can add the weighted compositions of binary eutectics as a candidate composition $C_{eutectic}$ for a multi-component alloy, which may be formulated as follows:

$$C_{eutectic} = \sum x_i C_{A_iB_i} \tag{1}$$

where $C_{eutectic}$ stands for the eutectic composition; A_i and B_i stand for the constituent element of the ith binary eutectic, while x_i is the weighting factor. Following this line of reasoning, many EHEAs or multi-component eutectic compositions were discovered, including $Nb_{0.45}CoCrFeNi$[57], $Nb_{0.8}Co_{1.74}Fe_{2.82}Ni$[60], $Nb_{0.5}CoFeNi$[84] and $Nb_{0.5}CoCrFeNi$[85,86], etc. Here we emphasized that the values of x_i are not fixed; however, in the literature, they were mostly set equal or nearly equal in a heuristic manner such that the overall composition was close to an equiatomic or near-equiatomic composition, as listed in Table 2.

Pseudo-binary eutectics

Since mixing of elements with a similar atomic size tends to form solid solutions[89,90], such as CoCrNi[91,92], CoCrFeNi[93], and $CoCrFeNi_2$[94], one alternative way to design EHEAs is to view these solid solutions as a

Table 2. EHEA compositions identified via Equation (1) compared with the experimental verifications

Alloy system	$C_{A_iB_i}$	x_i	$C_{eutectic}$ (calculated)	$C_{eutectic}$ (experimental)	Ref.
Nb-Co-Cr-Fe-Ni	$Nb_{13.9}Co_{86.1}$	0.25	$Nb_{0.6}CoCrFeNi$	$Nb_{0.45}CoCrFeNi$	[57]
	$Nb_{12}Cr_{88}$	0.25			
	$Nb_{10.6}Fe_{89.4}$	0.25			
	$Nb_{15.5}Ni_{84.5}$	0.25			
Ta-Co-Cr-Fe-Ni	Ta_8Co_{92}	0.25	$Ta_{0.47}CoCrFeNi$	$Ta_{0.4}CoCrFeNi$	[57]
	$Ta_{13}Cr_{87}$	0.25			
	$Ta_{7.5}Fe_{92.5}$	0.25			
	$Ta_{13.7}Ni_{86.3}$	0.25			
Zr-Co-Cr-Fe-Ni	$Zr_{9.5}Co_{90.5}$	0.25	$Zr_{0.51}CoCrFeNi$	$Zr_{0.55}CoCrFeNi$	[57]
	$Zr_{17.2}Cr_{82.8}$	0.25			
	$Zr_{9.8}Fe_{90.2}$	0.25			
	$Zr_{8.8}Ni_{91.2}$	0.25			
Hf-Co-Cr-Fe-Ni	$Hf_{11}Co_{89}$	0.25	$Hf_{0.49}CoCrFeNi$	$Hf_{0.4}CoCrFeNi$	[57]
	$Hf_{13}Cr_{87}$	0.25			
	$Hf_{7.9}Fe_{92.1}$	0.25			
	$Hf_{12.5}Ni_{87.5}$	0.25			
Nb-Co-Fe-Ni	$Nb_{13.9}Co_{86.1}$	0.29	$Nb_{0.62}Co_{1.22}Fe_{1.98}Ni$	$Nb_{0.62}Co_{1.22}Fe_{1.98}Ni$	[60]
	$Nb_{10.6}Fe_{89.4}$	0.46			
	$Nb_{15.5}Ni_{84.5}$	0.25			
Nb-Co-Fe-Ni	$Nb_{13.9}Co_{86.1}$	0.29	$Nb_{1.30}Co_{1.74}Fe_{2.82}Ni$	$Nb_{0.80}Co_{1.74}Fe_{2.82}Ni$	[60]
	$Nb_{10.6}Fe_{89.4}$	0.46			
	$Nb_{40.5}Ni_{59.5}$	0.25			
Zr-Co-Fe-Ni	$Zr_{9.5}Co_{90.5}$	0.29	$Zr_{0.43}Co_{1.19}Fe_{1.94}Ni$	$Zr_{0.53}Co_{1.19}Fe_{1.94}Ni$	[60]
	$Zr_{9.8}Fe_{90.2}$	0.47			
	$Zr_{8.8}Ni_{91.2}$	0.24			
Hf-Co-Fe-Ni	$Hf_{11}Co_{89}$	0.28	$Hf_{0.47}Co_{1.22}Fe_{2.11}Ni$	$Hf_{0.47}Co_{1.22}Fe_{2.11}Ni$	[60]
	$Hf_{7.9}Fe_{92.1}$	0.48			
	$Hf_{12.5}Ni_{87.5}$	0.24			
Nb-Co-Fe-Ni	$Nb_{13.9}Co_{86.1}$	0.33	$Nb_{0.49}CoFeNi$	$Nb_{0.5}CoFeNi$	[84]
	$Nb_{10.6}Fe_{89.4}$	0.33			
	$Nb_{15.5}Ni_{84.5}$	0.34			
Nb-Co-Cr-Fe-Ni	$Nb_{13.9}Co_{86.1}$	0.25	$Nb_{0.6}CoCrFeNi$	$Nb_{0.5}CoCrFeNi$	[85,86]
	$Nb_{12}Cr_{88}$	0.25			
	$Nb_{10.6}Fe_{89.4}$	0.25			
	$Nb_{15.5}Ni_{84.5}$	0.25			
Al_2O_3-Y_2O_3-ZrO_2	$(Al_2O_3)_{43}(Y_2O_3)_{57}$	0.35	$(Al_2O_3)_{44}(Y_2O_3)_{16}(ZrO_2)_{19}$	$(Al_2O_3)_{65}(Y_2O_3)_{16}(ZrO_2)_{19}$	[87]
	$(Al_2O_3)_{63}(ZrO_2)_{37}$	0.65			
Al_2O_3-Gd_2O_3-ZrO_2	$(Al_2O_3)_{77}(Gd_2O_3)_{23}$	0.57	$(Al_2O_3)_{102}(Gd_2O_3)_{19}(ZrO_2)_{23}$	$(Al_2O_3)_{58}(Gd_2O_3)_{19}(ZrO_2)_{23}$	[88]
	$(Al_2O_3)_{63}(ZrO_2)_{37}$	0.43			

"super element" and to substitute them for a normal element in a binary eutectic. In doing so, the candidate composition $C_{eutectic}$ may be expressed as:

$$C_{eutectic} \in [(C_I)_{1-x}(C_{II})_x],\ x \in (0,1) \tag{2}$$

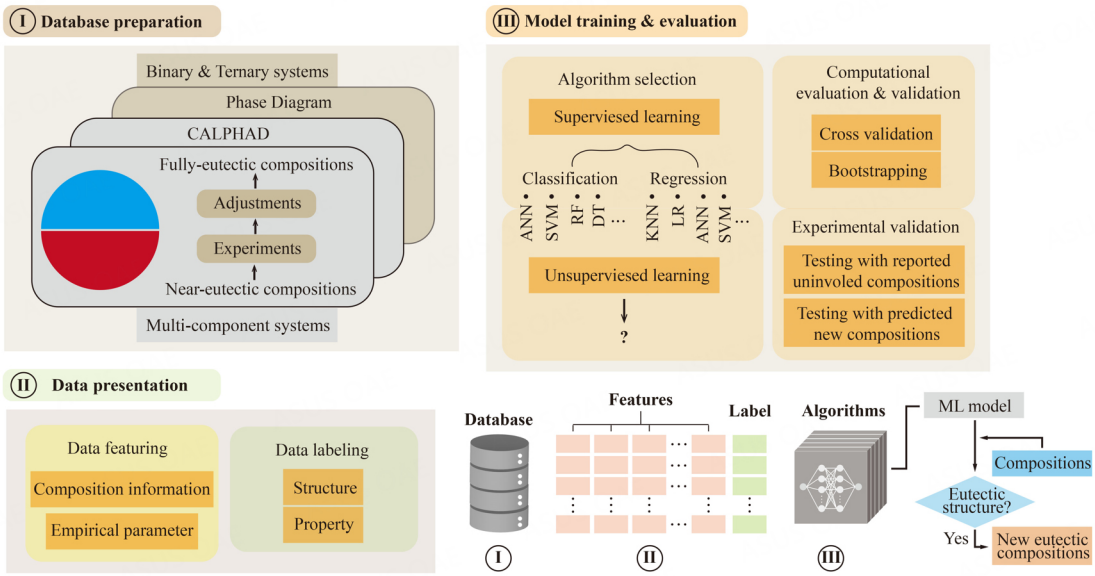

Figure 2. Schematic of a data-driven approach for the design of eutectic high entropy alloys.

where C_I denotes the "super element" (e.g., the mixture of elements that may form a solid solution) and C_{II} the single element in a pseudo-binary system. Following Equation (2), a number of EHEA compositions were discovered with the aid of CALPHAD[64-67,95-102], as tabulated in Table 3. Here, x is the composition yet to be determined via experiments or CALPHAD.

With CALPHAD, one can obtain the so-called pseudo-binary phase diagram as a function of x and temperature, through which fully-eutectic compositions can be identified, if any, for $C_{eutectic}$. For example, Wu *et al.*[109] identified the near-eutectic composition $Al_{19.4}Co_{20.6}Cr_{20.6}Ni_{39.4}$ for the pseudo-binary $(CoCrNi)_{1-x}(AlNi)_x$ alloy, which is very close to the eutectic composition of $Al_{17.4}Co_{21.7}Cr_{21.7}Ni_{39.2}$ verified experimentally. In light of the Scheil solidification theory, Yurchenko *et al.*[110] also successfully found the $Al_{28}Cr_{20}Nb_{15}Ti_{27}Zr_{10}$ EHEA. However, we note that all these above-mentioned methods are semi-empirical since CALPHAD is also based on the available database. Regardless of the difference in these methods, a more general method is always desirable, which can be applied to a wide range of compositions. In addition to the above-mentioned eutectic high entropy alloys, people also developed a number of eutectic refractory high entropy alloys[105-107], eutectic soldering high entropy alloys[108] and eutectic high entropy ceramics[87,88]. Interestingly, some of these eutectics could also be designed based on the aforementioned empirical rules. Therefore, we also list them in Tables 2 and 3 for the sake of completeness.

DATA-DRIVEN METHODS FOR THE DESIGN OF EUTECTIC HIGH ENTROPY ALLOYS

Database

In recent years, ML has been widely used to accelerate the search for advanced alloys[69-78]. As a data-driven approach, the performance of ML models is highly dependent on the quantity and quality of data[111,112]. Figure 2 illustrates the workflow of a typical ML approach to designing EHEAs. While EHEAs are important and very useful, we note that only a limited number of EHEA compositions are located out of vast compositional space with the ML approach [Table 4][79-81,113]. While one can easily find the data of binary and ternary eutectics from their corresponding phase diagrams, the data for EHEAs mainly comes from the literature, including those found through the empirical methods illustrated in Figure 1 and/or the results of CALPHAD calculations. Here, we note that the CALPHAD calculations are performed with

Table 3. EHEA compositions identified via Equation (2)

C_I	C_{II}	Parent binary eutectics	Pseudo-binary system	$C_{eutectic}$ (experimental)	Ref.
CoCrNi	Ta	(Co, Cr, Ni)-Ta	$(CoCrNi)_{1-x}Ta_x$	$CoCrNiTa_{0.4}$	[67]
	Nb	(Co, Cr, Ni)-Nb	$(CoCrNi)_{1-x}Nb_x$	$CoCrNiNb_{0.4}$	[100]
CoFeNi	NiAl	(Co, Ni)-Al	$(CoFeNi)_{1-x}(NiAl)_x$	$CoFeNi(NiAl)_{0.92}$	[101]
CoCrFeNi	Ta	(Co, Cr, Fe, Ni)-Ta	$(CoCrFeNi)_{1-x}Ta_x$	$CoCrFeNiTa_{0.75}$	[66]
				$CoCrFeNiTa_{0.43}$	[95]
	Nb	(Co, Cr, Fe, Ni)-Nb	$(CoCrFeNi)_{1-x}Nb_x$	$CoCrFeNiNb_{0.65}$	[64]
	Zr	(Co, Cr, Fe, Ni)-Zr	$(CoCrFeNi)_{1-x}Zr_x$	$CoCrFeNiZr_{0.5}$	[102]
	Hf	(Co, Cr, Fe, Ni)-Hf	$(CoCrFeNi)_{1-x}Hf_x$	$CoCrFeNiHf_{0.4}$	[103]
	Mo	(Co, Ni)-Mo	$(CoCrFeNi)_{1-x}Mo_x$	$CoCrFeNiMo_{0.8}$	[99]
$CoCrNi_2$	(V, B, Si)	(Co, Ni)-V (Co, Cr, Ni)-B (Co, Cr, Ni)-Si	$(CoCrNi_2)_{1-x}(V, B, Si)_x$	$CoCrNi_2(V_2B)_{0.43}$	[97]
				$CoCrNi_2(V_3B_2Si)_{0.2}$	[97]
$CoCrFeNi_2$	(V, B, Si)	(Co, Ni)-V (Co, Cr, Fe, Ni)-B (Co, Cr, Fe, Ni)-Si	$(CoCrFeNi_2)_{1-x}(V, B, Si)_x$	$CoCrFeNi_2(V_2B)_{0.51}$	[97]
				$CoCrNi_2(V_6B_3Si)_{0.149}$	[97]
	$Ni_{0.8}Al_{1.2}$	(Co, Fe, Ni)-Al	$(CoCrFeNi_2)_{1-x}(Ni, Al)_x$	$CoCrFeNi_2(Ni_{0.8}Al_{1.2})$	[65]
$Co_2CrFeNi$	$Ni_{0.8}Al_{1.2}$	(Co, Fe, Ni)-Al	$(Co_2CrFeNi)_{1-x}(Ni, Al)_x$	$Co_2CrFeNi(Ni_{0.8}Al_{1.2})$	[65]
$CoCrFe_2Ni$	$Ni_{0.8}Al_{1.2}$	(Co, Fe, Ni)-Al	$(CoCrFe_2Ni)_{1-x}(Ni, Al)_x$	$CoCrFe_2Ni(Ni_{0.8}Al_{1.2})$	[65]
Ni_2AlTi	V	Ni-V	$(Ni_2AlTi)_{1-x}V_x$	$(Ni_2AlTi)_{68}V_{32}$	[104]
CrNbTiZr	Al	(Nb, Zr)-Al	$(CrNbTiZr)_{1-x}Al_x$	$(CrNbTiZr)_{0.25}Al_{0.75}$	[105]
$HfMo_{0.5}NbTiV_{0.5}$	Si	(Hf, Mo, Nb, Ti, V)-Si	$(HfMo_{0.5}NbTiV_{0.5})_{1-x}Si_x$	-	[106]
HfCo	NbMo	Co-(Nb, Mo)	$(HfCo)_{1-x}(NbMo)_x$	$(HfCo)_{0.75}(NbMo)_{0.25}$	[107]
GaInSn	Zn	(Ga, In, Sn)-Zn	$(GaInSn)_{1-x}Zn_x$	-	[108]

Table 4. EHEA compositions identified via machine learning

Alloy	Database	Features	Label	Algorithm	Ref.
$Al_{18}Co_{30}Cr_{10}Fe_{10}Ni_{32}$	10 (Experiment) + 311(CALPHAD)	Compositions	Primary phase fraction	ANN	[79]
$Al_{19}Co_{16}Cr_{16}Ni_{49}$	4 (Experiment) + 96(CALPHAD)	Compositions	Primary phase fraction	SVM	[80]
$Hf_{0.34}Co_{1.33}Cr_{0.74}Fe_{0.20}Ni_{0.75}$	20 (Experiment)	Content of Co, Cr, Fe, Ni	Content of Hf	ELM	[81]
$Hf_{0.30}Co_{0.80}Cr_{1.40}Fe_{0.82}Ni_{0.16}$					
$Hf_{0.37}Co_{0.42}Cr_{0.81}Fe_{1.29}Ni_{0.82}$					
$Hf_{0.36}Co_{0.16}Cr_{0.76}Fe_{0.81}Ni_{1.38}$					
AlCrFe2.5Ni2.5 (Near-eutectic)	66 (Experiment)	Compositions, phase volume fractions	Melting range	GRNN	[113]

ANN: Artificial neural network; ELM: extreme learning machine; GRNN: generalized regression neural network; SVM: support vector machine.

respect to equilibrium phases, which might differ from the actual EHEA compositions that are metastable because of the fast cooling. In addition, one needs to be cautious while resorting to Scheil simulations for metastable phases, which are usually considered to represent as-cast phases[63,110,114,115] because it is performed by only considering atom diffusion in liquids (i.e. completely ignoring solid-state diffusion)[111].

To improve the data fidelity and also the performance of ML modeling, the data may need to be screened or pre-processed. Generally, data pre-processing includes (1) deletion of repetitive and incompatible data; (2) data normalization; and (3) data undersampling or oversampling[116-118]. However, randomly oversampling may result in model overfitting while randomly undersampling may cause loss of useful data, both of which

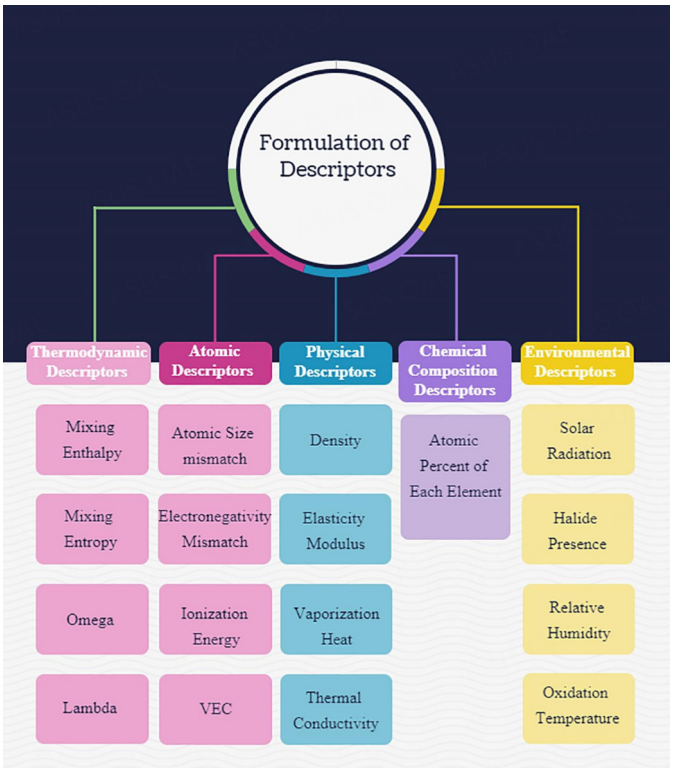

Figure 3. A typical categorization of data descriptors in the high entropy alloy design. Reproduced with permission from Roy *et al.*[124]. Copyright 2021, Elsevier.

could jeopardize the validity of the ML predictions[119]. Also, we note that metastability or the thermal history is another issue that may affect data fidelity. In such a case, one may obtain different microstructures and properties from the same alloy composition, such as $AlCoCrFeNi_3$ EHEA[120,121].

Data features & labels

After data collection, one needs to develop proper data features (or descriptors) and labels for the subsequent training of the ML models. Table 5 lists the commonly used features for the design of HEAs. Ideally, data features should be uncorrelated while containing all relevant information. In data-driven design of HEAs[122,123], alloy composition is usually the first data feature to be included. However, it is believed that only alloy composition alone is not sufficient. Therefore, other complementary data features, which are of physical relevance and significance, should be considered[112]. To date, nearly a hundred data features have been employed in the training and optimization of the ML models, which include the so-called atomic parameters[124-126], the environmental parameters[123], and the thermodynamic parameters which can all be derived from alloy composition[125-128], as represented in Figure 3 and Table 5.

The formulation of the complementary data features requires domain knowledge in material science and physical metallurgy[124]. To date, data features for eutectic alloys can be divided into two groups: (1) those related to eutectics formation and growth; and (2) those correlated with mechanical properties[1]. However, unlike the Hume-Rothery rules for solid solution HEAs[125,126,129], there still lacks a well-established general theory that can underpin the correlation between alloy compositions and eutectics, if there is any. Therefore, most ML models for EHEAs reported in the literature are solely based on the data feature of alloy composition [Table 4], which may compromise their performance. In practice, one can find the most important features using different approaches, such as Pearson Correlation Coefficient (PCC)[130,131] and

Table 5. List of the commonly used features of HEAs with the corresponding formula

	Data feature	Formula
Compositional feature	Molar fraction of components	c_i
Atomic features	Mean atomic radius	$a = \sum_{i=1}^{n} c_i r_i$
	Atomic size difference	$\delta = \sqrt{\sum_{i=1}^{n} c_i \left(1 - \frac{r_i}{a}\right)^2}$
	Valence electron concentration	$VEC = \sum_{i=1}^{n} c_i VEC_i$
	Electronegativity	$\chi = \sum_{i=1} c_i \chi_i$
Thermodynamic features	Mixing enthalpy	$\Delta H_{mix} = 4 \sum_{i \neq j} c_i c_j H_{ij}$
	Ideal mixing entropy	$S_{id} = -k_B \sum_{i=1}^{n} c_i ln c_i$
Physical features	Melting temperature	$T_m = \sum_{i=1}^{n} c_i T_{mi}$
	Elastic modulus	$E = \sum_{i=1}^{n} c_i E_i$
	Bulk modulus	$K = \sum_{i=1}^{n} c_i K_i$

Shapley Additive Explanation (SHAP) value[132]. We believe that data miners need to develop physics-informed data features, which can be derived from the fundamental theories for eutectic formation, such as the Jackson-Hunt theory[133], to improve the predictability of the machine learning models. At present, these are still the ongoing effort of active research for EHEAs. By comparison, the design of data labels for EHEAs is relatively more straightforward, which is either the characteristics of a eutectic-related microstructure (i.e., the volume fraction of eutectic phases[79,80]) or the targeted properties for regression ML modeling. For instance, Qiao *et al.*[113] used the difference between the solidus and liquidus temperature (i.e. the so-called melting range termed in Ref.[113]) as the data label, and the composition and phase fraction as the data feature in the search of EHEAs, which led to the discovery of a near-eutectic composition of $AlCrFe_{2.5}Ni_{2.5}$.

Machine learning model

After data are collected with their descriptors/labels being developed, the next task for the data-driven based alloy design is to select a proper ML algorithm. To date, there are a number of ML algorithms that have been used for the design of HEAs, such as support vector machine (SVM)[116,125,126,128,134], artificial neural network (ANN)[125,126,130,135], random forest (RF)[126,136,137], decision tree (DT)[138,139] and k-nearest neighbors (KNN)[130,140]. The selection of the ML algorithms can be either heuristic[116,141,142] or through benchmarking[125,135].

Once the ML algorithm is selected, the ML model will be trained and the reliability of the training results is usually evaluated against the issues, such as overfitting and underfitting, through cross-validation (CV)[143,144] and bootstrapping[122,131]. To be more specific, the testing accuracy[116,126], the Kappa index[128], the confusion matrix[118,145], and/or the receiver operating characteristic (ROC) curves[144] are usually used as the metric for the evaluation of classifiers, while the coefficient of determination (R^2)[146] and the root mean square error

Table 6. List of the ML models based on SVM or ANN with good performance on small-sized databases

Target	Size of database	Algorithm	Performance	Ref.
Phase prediction	118	ANN	Accuracy = 0.992	[127]
Phase prediction	401	ANN	Accuracy = 0.943	[130]
Phase prediction	550	SVM	Accuracy = 0.887	[134]
Phase prediction	322	SVM	Accuracy = 0.9384	[139]
Phase prediction	391	ANN	Accuracy = 0.92	[142]
Phase prediction	407	SVM	Accuracy = 0.9743	[149]
Phase prediction	209	ANN	Accuracy = 0.9297	[150]
Hardness prediction	155	SVM	RMSE = 31	[122]
Hardness prediction	214	SVM	R^2 = 0.873	[146]
Hardness prediction	370	SVM	R^2 = 0.8836	[147]
Hardness prediction	53	ANN	R^2 = 0.8575	[151]
Strength prediction	231	ANN	R^2 = 0.9702	[152]
EHEA Design	321	ANN	R^2 = 0.9663	[79]
EHEA Design	100	SVM	R^2 = 0.916	[80]

ANN: Artificial neural network; EHEA: Eutectic high entropy alloys; RMSE: root mean square error; SVM: support vector machine.

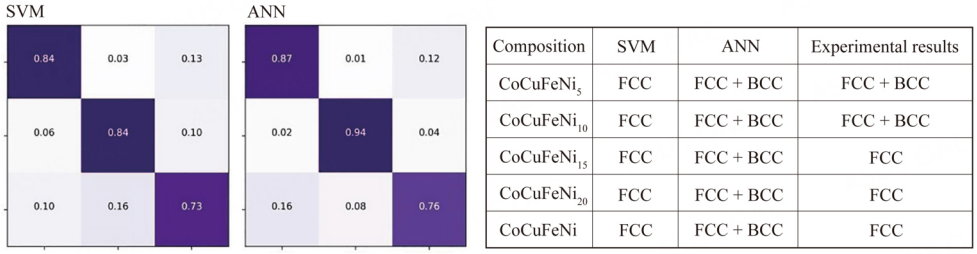

Figure 4. Confusion matrix of the SVM, ANN models, and the predicted results. Reproduced with permission from Jaiswal *et al.*[126]. Copyright 2021, Elsevier. ANN: artificial neural network; SVM: support vector machine.

(RMSE)[147] are usually used for regressors. It is noteworthy that the performance of the ML models should be judged not only by existing data (i.e. data in the database) but also by the "unseen" data (data out of the database). In addition to the above-mentioned numerical evaluations, experimental validation is therefore needed that produces unseen data to test the predictability of the ML models. For instance, Jaiswal *et al.*[126] used two different ML models (i.e., SVM and ANN) for the phase prediction of the $CoCuFeNi_x$ system. While both ML models achieve a similar numerical accuracy (~0.85), it appears that the ANN model can predict the result being consistent only with the experimental observation for low Ni content (x = 5, 10). In contrast, the SVM model can predict the results correctly only for high Ni content (x = 15, 20, 25), as illustrated in Figure 4.

Among the above-mentioned ML algorithms, the SVM and ANN are the ones that are widely used in the design of HEAs, including EHEAs, due to their good performance on small-sized databases[148], as shown in Table 6[79,80,122,127,130,134,139,142,146,147,149-152]. Here, we note that the reported ML models for EHEAs with good performance are mostly regressors, outperforming the classifier. This phenomenon could be attributed to the data imbalance in the EHEA database (i.e. the number of EHEAs is significantly smaller than that of non-eutectic HEAs)[153]. In practice, data shortage and/or imbalance could be an issue, particularly for the design of EHEAs. To mitigate the negative effect, people proposed a few methods, including (1) data rebalancing with the Synthetic Minority Oversampling Technique (SMOTE)[154] and the Tomek links for

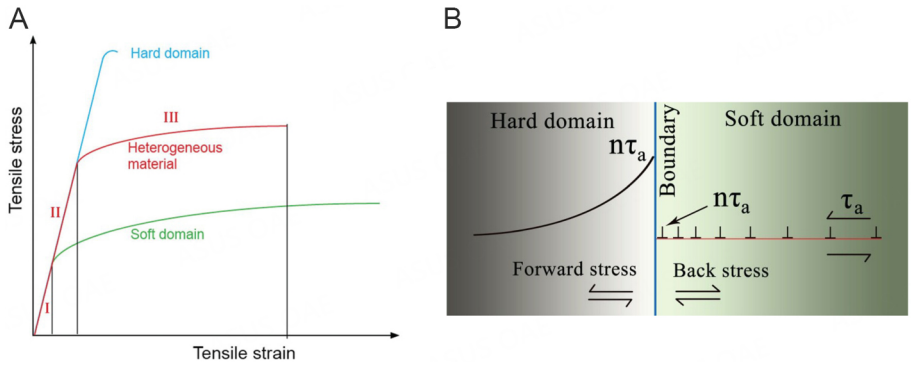

Figure 5. (A) Three-stage deformation of heterogeneous materials. Reproduced from Ref.[161]. CC BY 4.0; (B) schematic illustration of the heterogenous deformation strengthening mechanism. Reproduced from Ref.[162]. CC BY 4.0.

data cleaning[155]; (2) data augmentation with binary/ternary eutectics; (3) engineering of data features which may lead to improved predictability of the ML models even from the small dataset, such as Fuzzy C-means clustering function (FCM)[156] and Genetic Programming-based feature extraction using Rough Set Theory (GPRST)"[157]. In the literature, Bhowan *et al.*[158] proposed new parameters to mitigate the issue of imbalanced data. It includes (1) the average mean square error (*AMSE*), which uses the average *MSE* for each data class instead of the overall *MSE* for all data, (2) the incremental-reward-assigned accuracy (*Incr*), which can differentiate different models with similar accuracy by assigning a higher weighted factor to the outputs closer to the target value, and (3) the correlation-ratio-based parameter (*Corr*), which uses the separability of outputs for different data classes to evaluate the classifier performance. In our opinion, it is plausible to extend the finding of Bhowan *et al.* to the data-driven design of EHEAs, which, however, remains to be an open issue.

Currently, the design of eutectics is still limited in the dual-phase structure while only a few multi-phase eutectics were found, e.g. triple-phase eutectics[59], which makes the database significantly biased towards dual-phase eutectics and makes it difficult to find multi-phase eutectics using supervised machine learning models. To solve this problem, one method is to enlarge the database by including more multi-phase eutectics, which, however, is time-consuming. The other one is to use generative machine learning models, such as Variational Autoencoder (VAE)[159] or Generative Adversarial Network (GAN)[160], to generate multi-phase eutectics even with the data from binary eutectics. To our best knowledge, this has not been explored yet for EHEAs.

MECHANICAL PROPERTIES OF EUTECTIC HIGH ENTROPY ALLOYS

Similar to conventional eutectic alloys, EHEAs usually show lamellar or rod-like microstructure with alternating soft and hard phases. Such a heterogeneous microstructure (HS) can provide a unique strain hardening capability through the asynchronous plastic deformation of the soft and hard phases during plastic deformation, which is termed the heterogenous deformation induced (HDI) strengthening mechanism[161-163]. To rationalize the HDI effect, it was proposed that geometrically necessary dislocations (GNDs) will be generated during the plastic flow in a heterogeneous microstructure, which pile up along the interface between the hard/soft phase to maintain the overall deformation compatibility, as illustrated in Figure 5. As a result, this produces the back stress in the soft phase and forward stress in the hard phase, leading to the synergy that a more plastic flow is facilitated even at higher flow stress. Consequently, EHEAs usually show a balanced combination of strength and ductility, as shown in Figure 6[47,65,164-171]. To characterize the effect of HDI strengthening, various experimental techniques have been utilized, such as electron back scattered diffraction (EBSD)[172-174], transmission electron microscopy (TEM)[175,176], digital

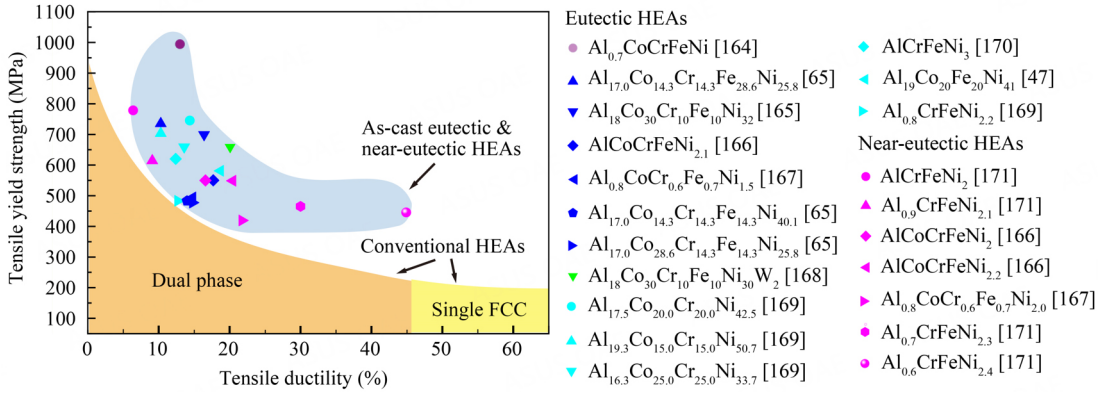

Figure 6. The superior mechanical properties of eutectic high entropy alloys overcome the strength-ductility trade-off in conventional high entropy alloys[47,65,164-171].

image correlation (DIC)[177] and the loading-unloading-reloading (LUR) tests[177,178], as illustrated in Figure 7.

In addition to the HDI strengthening, twinning-induced plasticity (TWIP) is another plausible strengthening mechanism in EHEAs, although, in the first place, it applies to materials of low stacking fault energy (SFE) with enhanced strain hardening capability and delayed plastic instability[179,180]. Through the so-called dynamic Hall-Petch effect, twin boundaries can act as obstacles to dislocation motion while permitting some partial dislocations to glide[181]. Diao *et al.*[182] reviewed the deformation twinning (DT) mechanism in HEAs and proposed the preferential conditions for the activation of the DT mechanism, including (a) large deformation strain; (b) low deformation temperature; (c) high strain rate; and (d) large grain size. With the first three conditions being met, a sufficient high dislocation density will be generated, leading to a high local stress for twin nucleation; while the last condition is to ensure there is sufficient space for high twinning activities (i.e. twin thickening)[183]. For instance, Shi *et al.*[180] uncovered a sequentially activated DT mechanism in the ultrafine-grained $Al_{19}Fe_{20}Co_{20}Ni_{21}$ EHEA which resulted in an outstanding combination of yield strength (~1.2 GPa) and tensile ductility (~24.0%).

Besides DT, transformation-induced plasticity (TRIP) is another strengthening mechanism that can be activated in an alloy with an even lower SFE[184]. For conventional HEAs, the deformation induced phase transformation can be activated by heuristically adjusting the alloy chemical composition to lower SFE[184,185]. However, it is difficult to activate or control the TRIP effect in EHEAs through compositional tuning because of the narrow compositional range for a eutectic alloy. Liu *et al.*[186] reported the phase transformation from the BCC/B2 phase to the FCC phase in the near-eutectic $AlCoFe_2Ni_2$ alloy and attributed this phenomenon to enhanced atom diffusion under high-temperature torsion. Wu *et al.*[187] found a phase transformation from B2 to BCT structure in the $Al_{18}Co_{30}Cr_{10}Fe_{10}Ni_{30}W_2$ EHEA during tensile deformation, which was thought to be responsible for the deformability of the B2 phase. These results are interesting and warrant further research. In particular, it still remains open whether EHEAs with the TRIP and/or TWIP effect can be designed through the aforementioned data-driven approach.

SUMMARY

To sum up, we provide a critical review of the recent development of EHEAs in this article by focusing on the various approach for compositional design, from the empirical to data-driven methods. Through the heuristic empirical methods based on binary eutectics (i.e., combination versus substitution), people have successfully developed a number of EHEAs; however, this trial-and-error approach is ineffective in

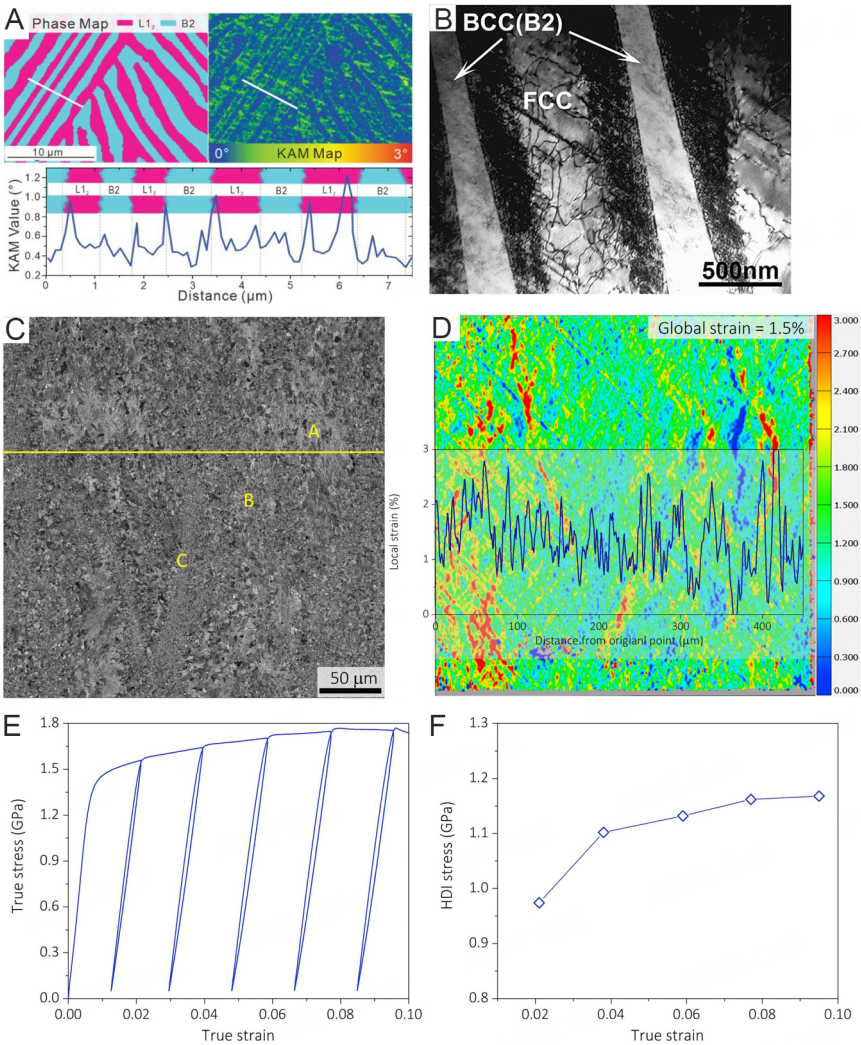

Figure 7. Characterization of heterogeneous deformation induced strengthening through various experimental techniques. (A) Phase map and kernel average misorientation map of electron back scattered diffraction (EBSD) results in the $Al_{19}Co_{20}Fe_{20}Ni_{41}$ EHEA. Reproduced from Ref.[173]. CC BY 4.0; (B) bright-field images of transmission electron microscopy (TEM) in the $AlCoCrFeNi_{2.1}$ EHEA. Reproduced with permission from Huang *et al.*[175]. Copyright 2021, Elsevier; (C) SEM image and (D) strain map of digital image correlation (DIC). A: deformed region; B: large grain; C: small grain; (E and F) loading-unloading-reloading (LUR) curves in the $Al_{0.2}CoCrFeNi_2Ti_{0.24}$ HEA. Reproduced with permission from He *et al.*[177]. Copyright 2021, Elsevier.

navigating the multi-dimensional compositional space. Therefore, people turned to the data-driven approach, such as ML modeling, which is supposed to be more effective in locating the eutectic compositions in the complex compositional space. However, the lack of sufficient high-fidelity EHEA data, the imbalanced database, and the poor design of data descriptors can compromise the performance of the ML models, which warrants further research efforts in this field. Finally, we also discuss the various strengthening mechanisms derived from the eutectic microstructure and compositional complexity in EHEAs (i.e., low stacking fault energy). These prior works indicate that the data-based design of EHEAs is promising but still at its infant stage.

DECLARATIONS

Author's contributions

Supervised the project: Yang Y

Wrote the manuscript: Chen Z, Yang Y

Availability of data and materials

Not applicable.

Financial support and sponsorship

The research of Yang Y is supported by the Research Grants Council (RGC), the Hong Kong government, through the General Research Fund (GRF) with account number (11201721) and by City University of Hong Kong through CityU Strategical Research Grants (7005933) and APRC-CityU new research initiatives/infrastructure support from central (9610603).

Conflicts of interest

Both authors declared that there are no conflicts of interest.

Ethical approval and consent to participate

Not applicable.

Consent for publication

Not applicable.

REFERENCES

1. Tiwary CS, Pandey P, Sarkar S, et al. Five decades of research on the development of eutectic as engineering materials. *Prog Mater Sci* 2022;123:100793. DOI
2. Chanda B, Potnis G, Jana PP, Das J. A review on nano-/ultrafine advanced eutectic alloys. *J Alloys Compd* 2020;827:154226. DOI
3. Kerr HW, Winegard WC. Solidification of eutectic alloys. *JOM* 1966;18:563-9. DOI
4. Dunlevey FM, Wallace JF. The effect of thermal cycling on the structure and properties of a Co, Cr, Ni-TaC directionally solidified eutectic alloy. *Metall Trans B* 1974;5:1351-6. DOI
5. Buchanan ER, Tarshis LA. Strengths and failure mechanisms of a Co-15Cr-13TaC directionally solidified eutectic alloy. *Metall Trans B* 1974;5:1413-22. DOI
6. Oishi K, Araki S, Terada Y. Effect of lamellar spacing on creep strength of α-Mg/C14-Mg_2Ca eutectic alloy. *Mater Trans* 2021;62:1414-9. DOI
7. El-ashram T, Shalaby RM. Effect of rapid solidification and small additions of Zn and Bi on the structure and properties of Sn-Cu eutectic alloy. *J Electron Mater* 2005;34:212-5. DOI
8. El-daly A, Hammad A. Enhancement of creep resistance and thermal behavior of eutectic Sn-Cu lead-free solder alloy by Ag and In-additions. *Mater Des* 2012;40:292-8. DOI
9. Liu Y, Michi RA, Dunand DC. Cast near-eutectic Al-12.5 wt.% Ce alloy with high coarsening and creep resistance. *Mater Sci Eng A* 2019;767:138440. DOI
10. Erol M, Keşlioğlu K, Şahingöz R, Maraşl N. Experimental determination of thermal conductivity of solid and liquid phases in Bi-Sn and Zn-Mg binary eutectic alloys. *Met Mater Int* 2005;11:421-8. DOI
11. Wang Z, Wang H, Yang M, et al. Thermal reliability of Al-Si eutectic alloy for thermal energy storage. *Mater Res Bull* 2017;95:300-6. DOI
12. Saheb N, Laoui T, Daud A, Harun M, Radiman S, Yahaya R. Influence of Ti addition on wear properties of Al-Si eutectic alloys. *Wear* 2001;249:656-62. DOI
13. Yasmin T, Khalid AA, Haque M. Tribological (wear) properties of aluminum-silicon eutectic base alloy under dry sliding condition. *J Mater Process Technol* 2004;153-154:833-8. DOI
14. Pashechko M, Lenik K. Segregation of atoms of the eutectic alloys Fe-Mn-C-B-Si-Ni-Cr at friction wear. *Wear* 2009;267:1301-4. DOI

15. Abouei V, Saghafian H, Shabestari S, Zarghami M. Effect of Fe-rich intermetallics on the wear behavior of eutectic Al-Si piston alloy (LM13). *Mater Des* 2010;31:3518-24. DOI
16. Yang J, Jeng S, Bain K, Amato R. Microstructure and mechanical behavior of in-situ directional solidified NiAl/Cr(Mo) eutectic composite. *Acta Mater* 1997;45:295-308. DOI
17. Caram R, Milenkovic S. Microstructure of Ni-Ni_3Si eutectic alloy produced by directional solidification. *J Cryst Growth* 1999;198-199:844-9. DOI
18. Kakitani R, de Gouveia GL, Garcia A, Cheung N, Spinelli JE. Thermal analysis during solidification of an Al-Cu eutectic alloy: interrelation of thermal parameters, microstructure and hardness. *J Therm Anal Calorim* 2019;137:983-96. DOI
19. Kamal M, El-blediwi AB, Karman MB. Structure, mechanical properties and electrical resistivity of rapidly solidified Pb-Sn-Cd and Pb-Bi-Sn-Cd alloys. *J Mater Sci Mater Electron* 1998;9:425-8. DOI
20. Liu CY, Chen C, Tu KN. Electromigration in Sn-Pb solder strips as a function of alloy composition. *J Appl Phys* 2000;88:5703-9. DOI
21. Feng W, Wang C, Morinaga M. Electronic structure mechanism for the wettability of Sn-based solder alloys. *J Electron Mater* 2002;31:185-90. DOI
22. Shangguan D, Achari A, Green W. Application of lead-free eutectic Sn-Ag solder in no-clean thick film electronic modules. *IEEE Trans Comp Packag Manuf Technol Part B* 1994;17:603-11. DOI
23. Gumaan MS, Shalaby RM, Ali EAM, Kamal M. Copper effects in mechanical, thermal and electrical properties of rapidly solidified eutectic Sn-Ag alloy. *J Mater Sci Mater Electron* 2018;29:8886-94. DOI
24. Shalaby RM. Development of holmium doped eutectic Sn-Ag lead-free solder for electronic packaging. *SSMT* 2022;34:277-86. DOI
25. Gogebakan M, Kursun C, Gunduz KO, Tarakci M, Gencer Y. Microstructural and mechanical properties of binary Ni-Si eutectic alloys. *J Alloys Compd* 2015;643:S219-25. DOI
26. Wei L, Zhao Z, Gao J, Cui K. Electrochemical production of a magnetic Ni_3Si template in lamellar Ni-Si eutectic alloy. *J Electrochem Soc* 2017;164:E332-6. DOI
27. Blaber MG, Engel CJ, Vivekchand SR, Lubin SM, Odom TW, Schatz GC. Eutectic liquid alloys for plasmonics: theory and experiment. *Nano Lett* 2012;12:5275-80. DOI PubMed
28. Yunusa M, Adaka A, Aghakhani A, et al. Liquid crystal structure of supercooled liquid gallium and eutectic gallium-indium. *Adv Mater* 2021;33:e2104807. DOI
29. Sheng LY, Nan L, Zhang W, Guo JT, Ye HQ. Microstructure and mechanical properties determined in compressive tests of quasi-rapidly solidified NiAl-Cr(Mo)-Hf eutectic alloy after hot isostatic pressure and high temperature treatments. *J Mater Eng Perform* 2010;19:732-6. DOI
30. Tang B, Cogswell DA, Xu G, Milenkovic S, Cui Y. The formation mechanism of eutectic microstructures in NiAl-Cr composites. *Phys Chem Chem Phys* 2016;18:19773-86. DOI PubMed
31. Senkov O, Miller J, Miracle D, Woodward C. Accelerated exploration of multi-principal element alloys for structural applications. *Calphad* 2015;50:32-48. DOI
32. Senkov ON, Miller JD, Miracle DB, Woodward C. Accelerated exploration of multi-principal element alloys with solid solution phases. *Nat Commun* 2015;6:6529. DOI PubMed PMC
33. Miracle D, Senkov O. A critical review of high entropy alloys and related concepts. *Acta Mater* 2017;122:448-511. DOI
34. Yeh J, Chen S, Lin S, et al. Nanostructured high-entropy alloys with multiple principal elements: novel alloy design concepts and outcomes. *Adv Eng Mater* 2004;6:299-303. DOI
35. Cantor B, Chang I, Knight P, Vincent A. Microstructural development in equiatomic multicomponent alloys. *Mater Sci Eng A* 2004;375-377:213-8. DOI
36. Yao M, Pradeep K, Tasan C, Raabe D. A novel, single phase, non-equiatomic FeMnNiCoCr high-entropy alloy with exceptional phase stability and tensile ductility. *Scr Mater* 2014;72-73:5-8. DOI
37. Kozak R, Sologubenko A, Steurer W. Single-phase high-entropy alloys - an overview. *Zeitschrift fur Krist* 2015;230:55-68. DOI
38. Laplanche G, Gadaud P, Horst O, Otto F, Eggeler G, George E. Temperature dependencies of the elastic moduli and thermal expansion coefficient of an equiatomic, single-phase CoCrFeMnNi high-entropy alloy. *J Alloys Compd* 2015;623:348-53. DOI
39. Maiti S, Steurer W. Structural-disorder and its effect on mechanical properties in single-phase TaNbHfZr high-entropy alloy. *Acta Mater* 2016;106:87-97. DOI
40. Shen J, Agrawal P, Rodrigues TA, et al. Microstructure evolution and mechanical properties in a gas tungsten arc welded $Fe_{42}Mn_{28}Co_{10}Cr_{15}Si_5$ metastable high entropy alloy. *Mater Sci Eng A* 2023;867:144722. DOI
41. Shen J, Gonçalves R, Choi YT, et al. Microstructure and mechanical properties of gas metal arc welded CoCrFeMnNi joints using a 308 stainless steel filler metal. *Scr Mater* 2023;222:115053. DOI
42. Tang Z, Senkov ON, Parish CM, et al. Tensile ductility of an AlCoCrFeNi multi-phase high-entropy alloy through hot isostatic pressing (HIP) and homogenization. *Mater Sci Eng A* 2015;647:229-40. DOI
43. Basu I, Ocelík V, De Hosson JTM. Size dependent plasticity and damage response in multiphase body centered cubic high entropy alloys. *Acta Mater* 2018;150:104-16. DOI
44. Manzoni AM, Glatzel U. New multiphase compositionally complex alloys driven by the high entropy alloy approach. *Mater Charact* 2019;147:512-32. DOI
45. Han L, Xu X, Li Z, Liu B, Liu CT, Liu Y. A novel equiaxed eutectic high-entropy alloy with excellent mechanical properties at

elevated temperatures. *Mater Res Lett* 2020;8:373-82. DOI

46. Dong Y, Lu Y, Kong J, Zhang J, Li T. Microstructure and mechanical properties of multi-component AlCrFeNiMox high-entropy alloys. *J Alloys Compd* 2013;573:96-101. DOI
47. Jin X, Zhou Y, Zhang L, Du X, Li B. A novel $Fe_{20}Co_{20}Ni_{41}Al_{19}$ eutectic high entropy alloy with excellent tensile properties. *Mater Lett* 2018;216:144-6. DOI
48. Vikram R, Gupta K, Suwas S. Design of a new cobalt base nano-lamellar eutectic high entropy alloy. *Scr Mater* 2021;202:113993. DOI
49. Wen X, Cui X, Jin G, Liu Y, Zhang Y, Fang Y. In-situ synthesis of nano-lamellar $Ni_{1.5}CrCoFe_{0.5}Mo_{0.1}Nb_x$ eutectic high-entropy alloy coatings by laser cladding: alloy design and microstructure evolution. *Surf Coatings Technol* 2021;405:126728. DOI
50. Shi P, Ren W, Zheng T, et al. Enhanced strength-ductility synergy in ultrafine-grained eutectic high-entropy alloys by inheriting microstructural lamellae. *Nat Commun* 2019;10:489. DOI PubMed PMC
51. Muskeri S, Hasannaeimi V, Salloom R, Sadeghilaridjani M, Mukherjee S. Small-scale mechanical behavior of a eutectic high entropy alloy. *Sci Rep* 2020;10:2669. DOI PubMed PMC
52. Lim X. Mixed-up metals make for stronger, tougher, stretchier alloys. *Nature* 2016;533:306-7. DOI PubMed
53. Jiang H, Qiao D, Lu Y, et al. Direct solidification of bulk ultrafine-microstructure eutectic high-entropy alloys with outstanding thermal stability. *Scr Mater* 2019;165:145-9. DOI
54. Yu Y, He F, Qiao Z, Wang Z, Liu W, Yang J. Effects of temperature and microstructure on the triblogical properties of CoCrFeNiNbx eutectic high entropy alloys. *J Alloys Compd* 2019;775:1376-85. DOI
55. Karati A, Guruvidyathri K, Hariharan V, Murty B. Thermal stability of AlCoFeMnNi high-entropy alloy. *Scr Mater* 2019;162:465-7. DOI
56. Shen J, Agrawal P, Rodrigues TA, et al. Gas tungsten arc welding of as-cast $AlCoCrFeNi_{2.1}$ eutectic high entropy alloy. *Mater Des* 2022;223:111176. DOI
57. Jiang H, Han K, Gao X, et al. A new strategy to design eutectic high-entropy alloys using simple mixture method. *Mater Des* 2018;142:101-5. DOI
58. Xie T, Xiong Z, Xu Z, Liu Z, Cheng X. Another eutectic point of Co-Cr-Fe-Ni-M (Hf, Ta, Nb) high-entropy system determined using a simple mixture method correlated with mixing enthalpy. *Mater Sci Eng A* 2021;802:140634. DOI
59. Jin X, Bi J, Liang Y, Qiao J, Li B. Triple-phase eutectic high-entropy alloy: $Al_{10}Co_{18}Cr_{18}Fe_{18}Nb_{10}Ni_{26}$. *Metall Mater Trans A* 2021;52:1314-20. DOI
60. Duan D, Wu Y, Chen H, et al. A strategy to design eutectic high-entropy alloys based on binary eutectics. *J Mater Sci Technol* 2022;103:152-6. DOI
61. He F, Wang Z, Ai C, Li J, Wang J, Kai J. Grouping strategy in eutectic multi-principal-component alloys. *Mater Chem Phys* 2019;221:138-43. DOI
62. Li T, Lu Y, Wang T, Li T. Grouping strategy *via* d-orbit energy level to design eutectic high-entropy alloys. *Appl Phys Lett* 2021;119:071905. DOI
63. Zhang L, Lu Y, Amar A, et al. Designing eutectic high-entropy alloys containing nonmetallic elements. *Adv Eng Mater* 2022;24:2200486. DOI
64. He F, Wang Z, Cheng P, et al. Designing eutectic high entropy alloys of $CoCrFeNiNb_x$. *J Alloys Compd* 2016;656:284-9. DOI
65. Jin X, Zhou Y, Zhang L, Du X, Li B. A new pseudo binary strategy to design eutectic high entropy alloys using mixing enthalpy and valence electron concentration. *Mater Des* 2018;143:49-55. DOI
66. Mukarram M, Mujahid M, Yaqoob K. Design and development of CoCrFeNiTa eutectic high entropy alloys. *J Mater Res Technol* 2021;10:1243-9. DOI
67. Huang T, Zhang J, Zhang J, Liu L. Effective design of Cr-Co-Ni-Ta eutectic medium entropy alloys with high compressive properties using combined CALPHAD and experimental approaches. *Appl Sci* 2021;11:6102. DOI
68. Ding Z, He Q, Yang Y. Exploring the design of eutectic or near-eutectic multicomponent alloys: from binary to high entropy alloys. *Sci China Technol Sci* 2018;61:159-67. DOI
69. Zou C, Li J, Wang WY, et al. Integrating data mining and machine learning to discover high-strength ductile titanium alloys. *Acta Mater* 2021;202:211-21. DOI
70. Nitol MS, Dickel DE, Barrett CD. Machine learning models for predictive materials science from fundamental physics: an application to titanium and zirconium. *Acta Mater* 2022;224:117347. DOI
71. Wang C, Fu H, Jiang L, Xue D, Xie J. A property-oriented design strategy for high performance copper alloys via machine learning. *NPJ Comput Mater* 2019:5. DOI
72. Zhang H, Fu H, Zhu S, Yong W, Xie J. Machine learning assisted composition effective design for precipitation strengthened copper alloys. *Acta Mater* 2021;215:117118. DOI
73. Zhao X, Huang H, Wen C, Su Y, Qian P. Accelerating the development of multi-component Cu-Al-based shape memory alloys with high elastocaloric property by machine learning. *Comput Mater Sci* 2020;176:109521. DOI
74. Singh R, Singh RP, Trehan R. Machine learning algorithms based advanced optimization of EDM parameters: an experimental investigation into shape memory alloys. *Sensors Int* 2022;3:100179. DOI
75. Hmede R, Chapelle F, Lapusta Y. Review of neural network modeling of shape memory alloys. *Sensors* 2022;22:5610. DOI PubMed PMC

76. Ward L, O'keeffe SC, Stevick J, Jelbert GR, Aykol M, Wolverton C. A machine learning approach for engineering bulk metallic glass alloys. *Acta Mater* 2018;159:102-11. DOI
77. Xiong J, Shi S, Zhang T. A machine-learning approach to predicting and understanding the properties of amorphous metallic alloys. *Mater Des* 2020;187:108378. DOI
78. Zhou ZQ, He QF, Liu XD, et al. Rational design of chemically complex metallic glasses by hybrid modeling guided machine learning. *NPJ Comput Mater* 2021:7. DOI
79. Wu Q, Wang Z, Hu X, et al. Uncovering the eutectics design by machine learning in the Al-Co-Cr-Fe-Ni high entropy system. *Acta Mater* 2020;182:278-86. DOI
80. Liu F, Xiao X, Huang L, Tan L, Liu Y. Design of NiCoCrAl eutectic high entropy alloys by combining machine learning with CALPHAD method. *Mater Today Commun* 2022;30:103172. DOI
81. Chen K, Xiong Z, An M, et al. Machine learning correlated with phenomenological mode unlocks the vast compositional space of eutectics of multi-principal element alloys. *Mater Des* 2022;219:110795. DOI
82. Agarwal R, Sonkusare R, Jha SR, Gurao N, Biswas K, Nayan N. Understanding the deformation behavior of CoCuFeMnNi high entropy alloy by investigating mechanical properties of binary ternary and quaternary alloy subsets. *Mater Des* 2018;157:539-50. DOI
83. Tsai M, Tsai R, Chang T, Huang W. Intermetallic phases in high-entropy alloys: statistical analysis of their prevalence and structural inheritance. *Metals* 2019;9:247. DOI
84. Ding Z, He Q, Wang Q, Yang Y. Superb strength and high plasticity in laves phase rich eutectic medium-entropy-alloy nanocomposites. *Int J Plast* 2018;106:57-72. DOI
85. Chung D, Ding Z, Yang Y. Hierarchical eutectic structure enabling superior fracture toughness and superb strength in $CoCrFeNiNb_{0.5}$ eutectic high entropy alloy at room temperature. *Adv Eng Mater* 2019;21:1801060. DOI
86. Ding Z, He Q, Chung D, Yang Y. Evading brittle fracture in submicron-sized high entropy intermetallics in dual-phase eutectic microstructure. *Scr Mater* 2020;187:280-4. DOI
87. Chen G, Fu X, Luo J, Zu Y, Zhou W. Effect of cooling rate on the microstructure and mechanical properties of melt-grown Al_2O_3/YAG/ZrO_2 eutectic ceramic. *J Eur Ceram Soc* 2012;32:4195-204. DOI
88. Liu H, Su H, Shen Z, et al. Direct formation of Al_2O_3/$GdAlO_3$/ZrO_2 ternary eutectic ceramics by selective laser melting: microstructure evolutions. *J Eur Ceram Soc* 2018;38:5144-52. DOI
89. He QF, Ye YF, Yang Y. The configurational entropy of mixing of metastable random solid solution in complex multicomponent alloys. *J Appl Phys* 2016;120:154902. DOI
90. He QF, Ding ZY, Ye YF, Yang Y. Design of high-entropy alloy: a perspective from nonideal mixing. *JOM* 2017;69:2092-8. DOI
91. Laplanche G, Kostka A, Reinhart C, Hunfeld J, Eggeler G, George E. Reasons for the superior mechanical properties of medium-entropy CrCoNi compared to high-entropy CrMnFeCoNi. *Acta Mater* 2017;128:292-303. DOI
92. Zhao P, Guan B, Tong Y, et al. A quasi-in-situ EBSD study of the thermal stability and grain growth mechanisms of CoCrNi medium entropy alloy with gradient-nanograined structure. *J Mater Sci Technol* 2022;109:54-63. DOI
93. Vaidya M, Guruvidyathri K, Murty B. Phase formation and thermal stability of CoCrFeNi and CoCrFeMnNi equiatomic high entropy alloys. *J Alloys Compd* 2019;774:856-64. DOI
94. He F, Wang Z, Wu Q, et al. Solid solution island of the Co-Cr-Fe-Ni high entropy alloy system. *Scr Mater* 2017;131:42-6. DOI
95. Ai C, He F, Guo M, et al. Alloy design, micromechanical and macromechanical properties of $CoCrFeNiTa_x$ eutectic high entropy alloys. *J Alloys Compd* 2018;735:2653-62. DOI
96. Rahul MR, Phanikumar G. Design of a seven-component eutectic high-entropy alloy. *Metall and Mat Trans A* 2019;50:2594-8. DOI
97. Zhang L, Lu Y, Amar A, et al. Eutectic high entropy alloys containing B and Si with excellent mechanical properties in annealing. *Mater Sci Eng A* 2022;856:143994. DOI
98. Chung D, Kwon H, Eze C, Kim W, Na Y. Influence of Ti addition on the strengthening and toughening effect in $CoCrFeNiTi_x$ multi principal element alloys. *Metals* 2021;11:1511. DOI
99. Guo Y, Liu L, Zhang Y, et al. A superfine eutectic microstructure and the mechanical properties of $CoCrFeNiMo_x$ high-entropy alloys. *J Mater Res* 2018;33:3258-65. DOI
100. Lu W, Luo X, Yang Y, Huang B. Effects of Nb additions on structure and mechanical properties evolution of CoCrNi medium-entropy alloy. *Mat Express* 2019;9:291-8. DOI
101. Zhang X, Chou T, Li W, Wang Y, Huang J, Cheng L. Microstructure and mechanical properties of $(FeCoNi)_{100-x}(NiAl)_x$ eutectic multi-principal element alloys. *J Alloys Compd* 2021;862:158349. DOI
102. Huo W, Zhou H, Fang F, Xie Z, Jiang J. Microstructure and mechanical properties of CoCrFeNiZrx eutectic high-entropy alloys. *Mater Des* 2017;134:226-33. DOI
103. Xie T, Xiong Z, Liu Z, Deng G, Cheng X. Excellent combination of compressive strength and ductility of (CoCrFeNi) ($Co_{0.26}Cr_{0.07}Fe_{0.16}Ni_{0.31}Hf_{0.4}$) high-entropy alloys. *Mater Des* 2021;202:109569. DOI
104. Wang M, Lu Y, Lan J, et al. Lightweight, ultrastrong and high thermal-stable eutectic high-entropy alloys for elevated-temperature applications. *Acta Mater* 2023;248:118806. DOI
105. Zhu M, Yao L, Liu Y, Zhang M, Li K, Jian Z. Microstructure evolution and mechanical properties of a novel $CrNbTiZrAl_x$ ($0.25 \leq x \leq 1.25$) eutectic refractory high-entropy alloy. *Mater Lett* 2020;272:127869. DOI
106. Liu Y, Zhang Y, Zhang H, et al. Microstructure and mechanical properties of refractory $HfMo_{0.5}NbTiV_{0.5}Si_x$ high-entropy

composites. *J Alloys Compd* 2017;694:869-76. DOI

107. Panina E, Yurchenko N, Tojibaev A, Mishunin M, Zherebtsov S, Stepanov N. Mechanical properties of $(HfCo)_{100-x}(NbMo)_x$ refractory high-entropy alloys with a dual-phase bcc-B2 structure. *J Alloys Compd* 2022;927:167013. DOI
108. Bai J, Wang Z, Zhang M, Qiao J. Effects of tailoring Zn additions on the microstructural evolution and electrical properties in $GaInSnZn_x$ high-entropy alloys. *Adv Eng Mater* 2023. DOI
109. Wu M, Wang S, Huang H, Shu D, Sun B. CALPHAD aided eutectic high-entropy alloy design. *Mater Lett* 2020;262:127175. DOI
110. Yurchenko N, Panina E, Zherebtsov S, Stepanov N. Design and characterization of eutectic refractory high entropy alloys. *Materialia* 2021;16:101057. DOI
111. Chen H, Mao H, Chen Q. Database development and Calphad calculations for high entropy alloys: challenges, strategies, and tips. *Mater Chem Phys* 2018;210:279-90. DOI
112. Zhou Z, Shang Y, Yang Y. A critical review of the machine learning guided design of metallic glasses for superior glass-forming ability. *J Mater Inf* 2022;2:2. DOI
113. Qiao L, Ramanujan R, Zhu J. Machine learning discovery of a new cobalt free multi-principal-element alloy with excellent mechanical properties. *Mater Sci Eng A* 2022;845:143198. DOI
114. Zhang C, Zhang F, Chen S, Cao W. Computational thermodynamics aided high-entropy alloy design. *JOM* 2012;64:839-45. DOI
115. Wei Q, Luo G, Zhang J, et al. Designing high entropy alloy-ceramic eutectic composites of $MoNbRe_{0.5}TaW(TiC)_x$ with high compressive strength. *J Alloys Compd* 2020;818:152846. DOI
116. Qu N, Chen Y, Lai Z, Liu Y, Zhu J. The phase selection via machine learning in high entropy alloys. *Procedia Manuf* 2019;37:299-305. DOI
117. Zhou Z, Zhou Y, He Q, Ding Z, Li F, Yang Y. Machine learning guided appraisal and exploration of phase design for high entropy alloys. *NPJ Comput Mater* 2019:5. DOI
118. Chang H, Tao Y, Liaw PK, Ren J. Phase prediction and effect of intrinsic residual strain on phase stability in high-entropy alloys with machine learning. *J Alloys Compd* 2022;921:166149. DOI
119. Batista GEAPA, Prati RC, Monard MC. A study of the behavior of several methods for balancing machine learning training data. *SIGKDD Explor Newsl* 2004;6:20-9. DOI
120. Zhu Z, Ma K, Wang Q, Shek C. Compositional dependence of phase formation and mechanical properties in three CoCrFeNi-(Mn/Al/Cu) high entropy alloys. *Intermetallics* 2016;79:1-11. DOI
121. Tian Q, Zhang G, Yin K, Cheng W, Wang Y, Huang J. Effect of Ni content on the phase formation, tensile properties and deformation mechanisms of the Ni-rich $AlCoCrFeNi_x$ (x = 2, 3, 4) high entropy alloys. *Mater Charact* 2021;176:111148. DOI
122. Wen C, Zhang Y, Wang C, et al. Machine learning assisted design of high entropy alloys with desired property. *Acta Mater* 2019;170:109-17. DOI
123. Dewangan SK, Kumar V. Application of artificial neural network for prediction of high temperature oxidation behavior of $AlCrFeMnNiW_x$ (x = 0, 0.05, 0.1, 0.5) high entropy alloys. *Int J Refract Met Hard Mater* 2022;103:105777. DOI
124. Roy A, Balasubramanian G. Predictive descriptors in machine learning and data-enabled explorations of high-entropy alloys. *Comput Mater Sci* 2021;193:110381. DOI
125. Krishna YV, Jaiswal UK, R RM. Machine learning approach to predict new multiphase high entropy alloys. *Scr Mater* 2021;197:113804. DOI
126. Jaiswal UK, Vamsi Krishna Y, Rahul M, Phanikumar G. Machine learning-enabled identification of new medium to high entropy alloys with solid solution phases. *Comput Mater Sci* 2021;197:110623. DOI
127. Islam N, Huang W, Zhuang HL. Machine learning for phase selection in multi-principal element alloys. *Comput Mater Sci* 2018;150:230-5. DOI
128. Machaka R. Machine learning-based prediction of phases in high-entropy alloys. *Comput Mater Sci* 2021;188:110244. DOI
129. Elton LRB. Atomic theory for students of metallurgy. *Phys Bull* 1960;11:309-309. DOI
130. Huang W, Martin P, Zhuang HL. Machine-learning phase prediction of high-entropy alloys. *Acta Mater* 2019;169:225-36. DOI
131. Chang Y, Jui C, Lee W, Yeh A. Prediction of the composition and hardness of high-entropy alloys by machine learning. *JOM* 2019;71:3433-42. DOI
132. Bundela AS, Rahul MR. Application of machine learning algorithms with and without principal component analysis for the design of new multiphase high entropy alloys. *Metall Mater Trans A* 2022;53:3512-9. DOI
133. Jackson K, Hunt J. Lamellar and rod eutectic growth. dynamics of curved fronts. Elsevier; 1988. pp. 363-76. DOI
134. Zhang Y, Wen C, Wang C, et al. Phase prediction in high entropy alloys with a rational selection of materials descriptors and machine learning models. *Acta Mater* 2020;185:528-39. DOI
135. Yan Y, Lu D, Wang K. Accelerated discovery of single-phase refractory high entropy alloys assisted by machine learning. *Comput Mater Sci* 2021;199:110723. DOI
136. Kaufmann K, Vecchio KS. Searching for high entropy alloys: a machine learning approach. *Acta Mater* 2020;198:178-222. DOI
137. Xiong J, Shi S, Zhang T. Machine learning of phases and mechanical properties in complex concentrated alloys. *J Mater Sci Technol* 2021;87:133-42. DOI
138. Bobbili R, Ramakrishna B, Madhu V. Development of machine learning based models for design of high entropy alloys. *Mater Technol* 2022;37:2580-7. DOI
139. Mandal P, Choudhury A, Mallick AB, Ghosh M. Phase prediction in high entropy alloys by various machine learning modules using

thermodynamic and configurational parameters. *Met Mater Int* 2023;29:38-52. DOI

140. Wang C, Zhong W, Zhao J. Insights on phase formation from thermodynamic calculations and machine learning of 2436 experimentally measured high entropy alloys. *J Alloys Compd* 2022;915:165173. DOI
141. Zeng Y, Man M, Bai K, Zhang Y. Revealing high-fidelity phase selection rules for high entropy alloys: a combined CALPHAD and machine learning study. *Mater Des* 2021;202:109532. DOI
142. Nassar A, Mullis A. Rapid screening of high-entropy alloys using neural networks and constituent elements. *Comput Mater Sci* 2021;199:110755. DOI
143. Schmidt J, Marques MRG, Botti S, Marques MAL. Recent advances and applications of machine learning in solid-state materials science. *NPJ Comput Mater* 2019:5. DOI
144. Pei Z, Yin J, Hawk JA, Alman DE, Gao MC. Machine-learning informed prediction of high-entropy solid solution formation: beyond the Hume-Rothery rules. *NPJ Comput Mater* 2020:6. DOI
145. Qu N, Liu Y, Zhang Y, et al. Machine learning guided phase formation prediction of high entropy alloys. *Mater Today Commun* 2022;32:104146. DOI
146. Bundela AS, Rahul M. Machine learning-enabled framework for the prediction of mechanical properties in new high entropy alloys. *J Alloys Compd* 2022;908:164578. DOI
147. Yang C, Ren C, Jia Y, Wang G, Li M, Lu W. A machine learning-based alloy design system to facilitate the rational design of high entropy alloys with enhanced hardness. *Acta Mater* 2022;222:117431. DOI
148. Tao Q, Xu P, Li M, Lu W. Machine learning for perovskite materials design and discovery. *NPJ Comput Mater* 2021:7. DOI
149. Zhang L, Chen H, Tao X, et al. Machine learning reveals the importance of the formation enthalpy and atom-size difference in forming phases of high entropy alloys. *Mater Des* 2020;193:108835. DOI
150. Chanda B, Jana PP, Das J. A tool to predict the evolution of phase and Young's modulus in high entropy alloys using artificial neural network. *Comput Mater Sci* 2021;197:110619. DOI
151. Jain R, Dewangan SK, Kumar V, Samal S. Artificial neural network approach for microhardness prediction of eight component FeCoNiCrMnVAlNb eutectic high entropy alloys. *Mater Sci Eng A* 2020;797:140059. DOI
152. Li J, Xie B, Fang Q, Liu B, Liu Y, Liaw PK. High-throughput simulation combined machine learning search for optimum elemental composition in medium entropy alloy. *J Mater Sci Technol* 2021;68:70-5. DOI
153. Kumar A, Goel S, Sinha N, Bhardwaj A. A review on unbalanced data classification. In: Uddin MS, Jamwal PK, Bansal JC, editors. Proceedings of International Joint Conference on Advances in Computational Intelligence. Singapore: Springer Nature; 2022. pp. 197-208. DOI
154. Chawla N V, Bowyer KW, Hall LO, Kegelmeyer WP. SMOTE: synthetic minority over-sampling technique. *J Artif Intell Res* 2002;16:321-57. DOI
155. Tomek I. Tomek link: two modifications of CNN. *IEEE Trans Syst Man Cybern* 1976;SMC-6:769-772. DOI
156. Lin KB, Weng W, Lai RK, Lu P. Imbalance data classification algorithm based on SVM and clustering function. *Proc 9th Int Conf Comput Sci Educ ICCCSE 2014* 2014:544-8. DOI
157. Moreno-Torres JG, Herrera F. A preliminary study on overlapping and data fracture in imbalanced domains by means of genetic programming-based feature extraction. *Proc 2010 10th Int Conf Intell Syst Des Appl ISDA'10* 2010:501-6. DOI
158. Bhowan U, Jahnston M, Zhang M. Developing new fitness functions in genetic programming for classification with unbalanced data. *IEEE Trans Syst Man Cybern Part B* 2012;42:406-21. DOI
159. Pei Z, Rozman KA, Doğan ÖN, et al. Machine-learning microstructure for inverse material design. *Adv Sci* 2021;8:e2101207. DOI PubMed PMC
160. Lee SY, Byeon S, Kim HS, Jin H, Lee S. Deep learning-based phase prediction of high-entropy alloys: optimization, generation, and explanation. *Mater Des* 2021;197:109260. DOI
161. Wu X, Zhu Y. Heterogeneous materials: a new class of materials with unprecedented mechanical properties. *Mater Res Lett* 2017;5:527-32. DOI
162. Zhu Y, Wu X. Perspective on hetero-deformation induced (HDI) hardening and back stress. *Mater Res Lett* 2019;7:393-8. DOI
163. Sathiyamoorthi P, Kim HS. High-entropy alloys with heterogeneous microstructure: Processing and mechanical properties. *Prog Mater Sci* 2022;123:100709. DOI
164. Gwalani B, Gangireddy S, Zheng Y, Soni V, Mishra RS, Banerjee R. Influence of ordered L1(2) precipitation on strain-rate dependent mechanical behavior in a eutectic high entropy alloy. *Sci Rep* 2019;9:6371. DOI PubMed PMC
165. Yang Z, Wang Z, Wu Q, et al. Enhancing the mechanical properties of casting eutectic high entropy alloys with Mo addition. *Appl Phys A* 2019:125. DOI
166. Lu Y, Gao X, Jiang L, et al. Directly cast bulk eutectic and near-eutectic high entropy alloys with balanced strength and ductility in a wide temperature range. *Acta Mater* 2017;124:143-50. DOI
167. Ma L, Wang J, Jin P. Microstructure and mechanical properties variation with Ni content in $Al_{0.8}CoCr_{0.6}Fe_{0.7}Ni_x$ (x = 1.1, 1.5, 1.8, 2.0) eutectic high-entropy alloy system. *Mater Res Express* 2020;7:016566. DOI
168. Wu Q, Wang Z, Zheng T, et al. A casting eutectic high entropy alloy with superior strength-ductility combination. *Mater Lett* 2019;253:268-71. DOI
169. Liu Q, Liu X, Fan X, et al. Designing novel AlCoCrNi eutectic high entropy alloys. *J Alloys Compd* 2022;904:163775. DOI
170. Dong Y, Yao Z, Huang X, et al. Microstructure and mechanical properties of $AlCo_xCrFeNi_{3-x}$ eutectic high-entropy-alloy system. *J*

Alloys Compd 2020;823:153886. DOI
171. Jin X, Bi J, Zhang L, et al. A new $CrFeNi_2Al$ eutectic high entropy alloy system with excellent mechanical properties. *J Alloys Compd* 2019;770:655-61. DOI
172. Shi P, Li R, Li Y, et al. Hierarchical crack buffering triples ductility in eutectic herringbone high-entropy alloys. *Science* 2021;373:912-8. DOI
173. Li Y, Shi P, Wang M, et al. Unveiling microstructural origins of the balanced strength-ductility combination in eutectic high-entropy alloys at cryogenic temperatures. *Mater Res Lett* 2022;10:602-10. DOI
174. An Z, Mao S, Liu Y, et al. Inherent and multiple strain hardening imparting synergistic ultrahigh strength and ductility in a low stacking faulted heterogeneous high-entropy alloy. *Acta Mater* 2023;243:118516. DOI
175. Huang L, Sun Y, Chen N, et al. Simultaneously enhanced strength-ductility of $AlCoCrFeNi_{2.1}$ eutectic high-entropy alloy via additive manufacturing. *Mater Sci Eng A* 2022;830:142327. DOI
176. Chen X, Kong J, Li J, et al. High-strength $AlCoCrFeNi_{2.1}$ eutectic high entropy alloy with ultrafine lamella structure via additive manufacturing. *Mater Sci Eng A* 2022;854:143816. DOI
177. He F, Yang Z, Liu S, et al. Strain partitioning enables excellent tensile ductility in precipitated heterogeneous high-entropy alloys with gigapascal yield strength. *Int J Plast* 2021;144:103022. DOI
178. Song SC, Moon J, Kim HS. Hetero-deformation-induced strengthening of multi-phase Cu-Fe-Mn medium entropy alloys by dynamic heterostructuring. *Mater Sci Eng A* 2021;799:140275. DOI
179. Chen L, Zhao Y, Qin X. Some aspects of high manganese twinning-induced plasticity (TWIP) steel, a review. *Acta Metall Sin* 2013;26:1-15. DOI
180. Shi P, Zhong Y, Li Y, et al. Multistage work hardening assisted by multi-type twinning in ultrafine-grained heterostructural eutectic high-entropy alloys. *Mater Today* 2020;41:62-71. DOI
181. Laplanche G, Kostka A, Horst O, Eggeler G, George E. Microstructure evolution and critical stress for twinning in the CrMnFeCoNi high-entropy alloy. *Acta Mater* 2016;118:152-63. DOI
182. Diao H, Feng R, Dahmen K, Liaw P. Fundamental deformation behavior in high-entropy alloys: an overview. *Curr Opin Solid State Mater Sci* 2017;21:252-66. DOI
183. Wu SW, Wang G, Yi J, et al. Strong grain-size effect on deformation twinning of an $Al_{0.1}CoCrFeNi$ high-entropy alloy. *Mater Res Lett* 2017;5:276-83. DOI
184. Liu S, Wu Y, Wang H, et al. Transformation-reinforced high-entropy alloys with superior mechanical properties via tailoring stacking fault energy. *J Alloys Compd* 2019;792:444-55. DOI
185. Li Z, Chen L, Fu P, Su H, Dai P, Tang Q. The effect of Si addition on the heterogeneous grain structure and mechanical properties of CrCoNi medium entropy alloy. *Mater Sci Eng A* 2022;852:143655. DOI
186. Liu X, Ding H, Huang Y, et al. Evidence for a phase transition in an $AlCrFe_2Ni_2$ high entropy alloy processed by high-pressure torsion. *J Alloys Compd* 2021;867:159063. DOI
187. Wu Q, He F, Li J, Kim HS, Wang Z, Wang J. Phase-selective recrystallization makes eutectic high-entropy alloys ultra-ductile. *Nat Commun* 2022;13:4697. DOI PubMed PMC